HHS Public Access

Author manuscript

Exp Eye Res. Author manuscript; available in PMC 2022 June 01.

Published in final edited form as:

Exp Eye Res. 2021 June ; 207: 108579. doi:10.1016/j.exer.2021.108579.

Temporal Evolution of the Biological Response to Laser-Induced Refractive Index Change (LIRIC) in Rabbit Corneas

Kaitlin T. Wozniak[1,2,3], **Sam C. Butler**[4], **Xu He**[3], **Jonathan D. Ellis**[4], **Wayne H. Knox**[1,2], **Krystel R. Huxlin**[1,2,3]

[1]The Institute of Optics, University of Rochester, Rochester, NY 14627, USA

[2]The Center for Visual Science, University of Rochester, Rochester, NY 14627, USA

[3]The Flaum Eye Institute, University of Rochester, Rochester, NY 14642, USA

[4]Clerio Vision Inc., Rochester, NY 14618, USA

Abstract

Laser induced refractive index change (LIRIC) is a new, non-incisional, non-ablative, femtosecond photo-modification technique being developed for vision correction in humans. Prior, *ex-vivo* studies showed intra-tissue refractive index change to induce minimal cell death, restricted to the laser focal zone in the corneal stroma, and with no observable damage to the epithelium or endothelium. Here, we used live rabbits to ascertain longer-term consequences of LIRIC *in vivo.* Specifically, we assessed cell death, fibrosis, corneal nerve distribution, endothelial cell density, and corneal structure for up to 3 months after LIRIC. A +2.5 D gradient-index LIRIC Fresnel lens was inscribed inside 20 applanated corneas of Dutch-Belted rabbits, over a circular region of the mid-stroma measuring 4.5 mm in diameter. Twelve additional rabbit eyes were used as applanation-only controls to differentiate the effects of laser treatment and suction applanation on biological and structural parameters. *In vivo* optical measurements were performed pre-operatively, then immediately, 2, 4, and 12 weeks after the procedure, to measure endothelial cell density and changes in corneal structure. Groups of four rabbits were sacrificed at 4 hours, 2, 4, and 12 weeks after LIRIC for histological determinations; the TUNEL assay was used to evaluate cell death, H&E staining was used to assess inflammatory infiltration, and immunostaining for α-smooth muscle actin (α-SMA) and βIII tubulin (Tuj-1) was performed to assess myofibroblast differentiation and corneal nerve distribution, respectively. Consistent with prior *ex vivo* data, only minimal cell death was observed in the laser focal zone, with TUNEL-positive cells restricted to the stromal region of refractive index change 4 hours after LIRIC. No TUNEL-positive cells were evident anywhere in the cornea 2, 4, or 12 weeks after LIRIC. Applanation-only corneas were

Correspondence: Krystel R. Huxlin, PhD, Flaum Eye Institute, University of Rochester, 601 Elmwood Ave, Box 314, Rochester, NY 14642, USA. Phone +1-(585) 275-5495; khuxlin@ur.rochester.edu.

The authors declare the following interests: Huxlin, Knox, Ellis and Butler have equity in Clerio Vision, Inc., which partially supported this research. At the time when this work was performed, Huxlin, Knox and Ellis had no fiduciary responsibility in Clerio Vision, Inc. Ellis and Butler are currently employed by Clerio Vision, Inc.

completely TUNEL-negative. Neither LIRIC-treated nor applanation-only eyes exhibited α-SMA-positive staining or altered corneal nerve distributions at any of the time points examined. *In vivo* confocal imaging revealed normal endothelial cell densities in all eyes (whether LIRIC-treated or applanation-only) at all time points. Optical coherence tomography showed suction applanation to cause a temporary decrease in central corneal thickness, which returned to normal within four hours. Corneas into which Fresnel LIRIC lenses were written while applanated did not undergo major structural or shape changes beyond the temporary thinning already described for suction applanation. The present findings suggest that LIRIC patterns, which generated a clinically-relevant refractive correction in the mid-stromal region of live rabbit corneas, induced little-to-no disruption to corneal structure and biology for 3 months after the procedure. This affirms the relative safety of LIRIC and predicts that compared to traditional laser vision correction surgeries, common post-operative complications such as dry eye, haze, or patient discomfort may be entirely avoided.

Keywords

refractive surgery; stroma; TUNEL; wound healing; myofibroblasts; corneal nerves; corneal endothelial cells

1 Introduction

The wound healing response and post-operative complications that can follow laser refractive procedures such as laser in-situ keratomileusis (LASIK) and photorefractive keratectomy (PRK) have been studied extensively. A small percentage of patients develop post-operative stromal haze (Spadea *et al.*, 2016), discomfort (Shortt *et al.*, 2013; Torres *et al.*, 2007), and optical side effects such as glare and halos (Chan and Manche, 2011; Peng *et al.*, 2018), likely arising from disruption of the epithelial-stromal interface, keratocyte apoptosis (Torricelli *et al.*, 2016; Wilson, 2020b), myofibroblast differentiation (Bühren *et al.*, 2009; Wilson, 2020a), and other wound-healing associated remodeling (Nakamura *et al.*, 2001). In addition, corneal nerves are damaged in LASIK and PRK due to flap creation (LASIK), epithelial debridement (PRK) and stromal photoablation (both LASIK and PRK); this can lead to long-term complications such as dry eye (Ambrósio Jr *et al.*, 2008; Hindman *et al.*, 2019; Jeon *et al.*, 2018; Kauffmann *et al.*, 1996; Patel and Erie, 2003; Shaheen *et al.*, 2014).

In 2008, our group began work on a femtosecond-laser-based procedure, which we termed intra-tissue refractive index shaping (IRIS). The ability to use this laser modality for refractive index (RI) change was originally demonstrated in hydrogels (Ding *et al.*, 2006) and was first attempted in cornea using an 800 nm femtosecond laser system (Ding *et al.*, 2008). We subsequently showed that this novel, multi-photon technique was more efficient at locally increasing the RI of corneal stromal tissue when using a tightly-focused, 400 nm femtosecond laser with a high repetition rate (Xu *et al.*, 2011). This allowed us to inscribe small (2.5 mm wide) gradient index (GRIN) lenses of positive RI change in the corneas of behaviorally-trained cats, and to show that this process induced measurable levels of wavefront change (Savage *et al.*, 2014). Importantly, induced optical changes were stable for

up to 18 months (Savage *et al.*, 2014), raising questions about the biological impact of this novel procedure. In *ex vivo* cat corneas, IRIS induced significantly less cell death than femto-LASIK, and dying cells were largely restricted to regions of RI change, with no cell damage seen in distant portions of the stroma, in the overlying epithelium, or underlying endothelium (Wozniak *et al.*, 2017).

More recently, our team developed IRIS into a non-ablative, non-incisional, laser refractive correction procedure for human applications, naming it laser-induced refractive index change (LIRIC). LIRIC was first successfully tested in humans in 2019 by inscribing a small (3mm diameter) gradient index (GRIN) lens in the corneal mid-stroma (Zheleznyak *et al.*, 2019). However, long-term biological consequences of LIRIC have yet to be assessed. For instance, we do not know if the minimal cell death observed following inscription of small area (2–3 mm diameter) LIRIC GRIN lenses into *ex-vivo* corneas (Wozniak *et al.*, 2017) holds when larger (4–6 mm diameter) LIRIC GRIN lenses are inscribed into living animals (or humans). Knowing how much damage is induced and to what corneal elements, is an important determinant of possible complications. Together with the lack of epithelial flap creation, if *in vivo* LIRIC also caused minimal cell death, this could limit the wound healing response. As such, LIRIC could cause fewer side-effects than traditional laser refractive surgeries. The present investigation tested this hypothesis and assessed the impact of LIRIC both qualitatively and quantitatively, using a combination of *in vivo* imaging techniques and histology. Importantly, this was done in live rabbits over a 12-week, post-procedural time period.

2 Methods

2.1 LIRIC instrumentation and procedure

The femtosecond laser system employed here (Fig. 1A) was previously described (Wozniak *et al.*, 2018). In brief, RI change was achieved by scanning the focal volume of a 405 nm, femtosecond laser through each cornea. Here, we used a mode-locked Ti:Sapphire oscillator (Mai Tai HP, Spectra Physics Corporation, Santa Clara, CA) which generated up to 3 W of 810 nm, 100 fs pulses at an 80 MHz repetition rate. The light was frequency doubled to 405 nm through second harmonic generation (SHG). Active laser intensity control was achieved by focusing the laser light through an acousto-optic modulator (AOM - M113-aQ80L-2; Isomet Corp., Old Town Manassas, VA). The first order diffracted beam was selected, and the laser intensity was modulated via a voltage signal to the AOM driver with megahertz bandwidth (Brooks *et al.*, 2014). The AOM was synchronized to the scanning system in order to control the magnitude of RI change along scanned, GRIN lines. The pulse width was dispersion-compensated by two Gires-Tournois interferometric (GTI) mirrors (Layertec, Mellingen, Germany) to ~165 fs in the focal volume. A 2D, orthogonal mirror galvanometer (AGV-14HPO; Aerotech, Inc., Pittsburgh, PA) steered the beam, and a Galilean beam expander controlled the effective numerical aperture (NA) of the system by adjusting the size of the beam on the entrance pupil of the microscope objective. An effective NA of 0.53 was used in the present experiments. Finally, the beam was relayed through a unit magnification Keplerian telescope to the focusing microscope objective. The galvanometer scanned the focal volume through the field of view (FOV) of the objective as two linear

stages (ANT130L-060; Aerotech, Inc., Pittsburgh, PA) translated the focusing objective above the stationary cornea, creating a raster scan pattern with uniform line spacing. This scanning system allowed for high speed writing of small area GRIN structures in the cornea that were then stitched together to compose the final Fresnel lens (Fig. 1B, C). The dimensions of this Fresnel lens were chosen to be clinically relevant, with a large area (4.5 mm diameter), an optically-meaningful refractive prescription (+2.5 D), and positioning in the anterior 1/3 of the cornea. The 4.5 mm diameter optical zone was limited by the size of the rabbit cornea, which is significantly smaller than a human cornea.

We note here that for refractive corrections, it is more practical to discuss the accumulated optical phase of a wavefront, rather than RI change *per se,* with the relationship between phase and RI defined as

$$\Delta\varphi = \frac{2\pi b \Delta n}{\lambda}, \quad (1)$$

where $\Delta\varphi$ is the induced phase, b is the thickness of the region of RI change, Δn is the magnitude of RI change, and λ is the measurement wavelength of the induced phase. Prior to performing LIRIC *in vivo*, we measured the amount of induced phase change in three *ex vivo* Dutch Belted rabbit corneas using previously-described methods (Gandara-Montano *et al.*, 2015; Gandara-Montano *et al.*, 2017). This allowed us to establish that 200 mW - the maximum laser power delivered in our single-layer, GRIN Fresnel lenses - induced 0.28 ± 0.11 waves of change when measured at 535 nm (Fig. 1C).

2.2 Animal procedures

Sixteen young, female, Dutch-Belted rabbits were obtained from Covance Research Products (Denver, PA). Dutch-Belted rabbits were preferred for this study because like most humans, they have pigmented irises and display more genetic variability than New Zealand White rabbits. All animal procedures were conducted according to the guidelines of the ARVO Statement for the Use of Animals in Ophthalmic and Vision Research and the NIH Guide for the Care and Use of Laboratory Animals.

During the LIRIC procedure, each animal was anesthetized with intramuscular ketamine (20 mg/kg) + dexmedetomidine hydrochloride (0.15 mg/kg) prior to being aligned beneath the microscope objective (Fig. 1D). In accordance with human laser eye procedures, the rabbits' pupils were dilated prior to treatment (topical tropicamide 1% and phenylephrine 2.5%, Akorn, Lake Forest, IL), and they received a topical anesthetic (0.5% proparacaine, Sandoz/Falcon Pharma Ltd., Fort Worth, TX). To keep the rabbit's eye hydrated, the cornea was lubricated using hydroxypropyl methylcellulose-sodium perborate eye gel (GenTeal, Alcon Inc., Geneva, Switzerland).

To perform LIRIC, each cornea was flat-applanated using a custom-built device consisting of a ~170 μm-thick glass window with a 6 mm diameter clear aperture mounted on a polycarbonate ring with an annular suction ring that fit inside the rabbit's orbit. A spring-loaded syringe was connected to the suction ring and used to draw suction. In this manner, the applanator maintained constant suction around the scleral edge and immobilized the eye

during the LIRIC writing process. Once the rabbit was mounted onto the suction ring, the microscope objective was lowered into the patient interface (Fig. 1D), and the LIRIC laser treatment began. A scan speed of 220 mm/s and a line spacing of 0.5 μm were used to minimize applanation times while maximizing LIRIC's efficacy. The average (± SD) applanation time for the entire LIRIC procedure was 8.0 ± 1.1 minutes. It should be noted that this is longer than would optimally be used in human patients. In fact, recent improvements to the laser scanning system for creating LIRIC refractive correctors in patients have decreased writing times and allowed our team to create presbyopic correctors in 82 seconds (Zheleznyak *et al.*, 2019).

Another relevant outcome was the location of the LIRIC patterns in the cornea. Patterns were sometimes displaced towards the temporal side of the rabbits' eyes. This was likely due to the mounting of the rabbit's head in the LIRIC system during anesthesia: animals were laid on their side, and in some cases, the rabbits' eyes rolled in their orbit toward their nose, making the temporal region more central relative to the applanator. For vision correction in humans, when patients are awake and able to fixate a visual target, LIRIC patterns have been and will continue to be centered on the pupil (Zheleznyak *et al., 2019*).

Twenty eyes underwent the LIRIC procedure. The remaining 12 eyes were applanation-only Shams, allowing us to differentiate the impact of laser treatment and suction applanation. Sham eyes were treated identically to LIRIC eyes, except that there was no laser exposure. One of the Sham treatments was unsuccessful: this rabbit was the smallest of the cohort, and while we were able to carry out the LIRIC procedure in her first eye, the applanator ring was oversized for the orbital space of her second eye, causing suction-applanation to fail. Therefore, the total number of analyzable Sham eyes was reduced to eleven.

2.3 In vivo optical measurements

Two types of *in vivo* optical measurements were performed to investigate the biological impact of LIRIC and applanation on the rabbit cornea. OCT was used to measure corneal thickness, and confocal imaging was used to measure central endothelial cell density. Both were performed three times per rabbit: 2 weeks prior to LIRIC (baseline), immediately post-treatment, and pre- sacrifice at either 4 hours, 2 weeks, 4 weeks, or 12 weeks post-treatment.

OCT imaging—was performed *in vivo* using a Bioptigen SD-OCT (Leica, Wetzlar, Germany). Awake rabbits were gently restrained while each eye was lubricated using GenTeal gel and aligned to the OCT probe. The OCT collected 75 frames over a 6 mm by 2 mm rectangular scan, 25 frames in 3 different slices along the superior-inferior axis. The LIRIC pattern was visible in OCT images as a thin region of increased reflectivity (Fig. 2A). After the pattern was located in one of the OCT image stacks (the three slices along the superior-inferior axis), 5 to 10 images per eye were analyzed (total of 870 images) using a custom MATLAB program. To measure corneal thickness, the user selects points along the anterior and posterior corneal surfaces to define the best fit circle (BFC) which determined the radius of curvature (ROC). The program then finds a vector normal to the anterior surface, and the distance to the intersection between this vector and the second surface is then solved analytically. Two different types of thickness measurements were extracted from

each OCT image (Fig. 2A): central corneal thickness (CCT) and peripheral corneal thickness (PCT). The latter was necessary because LIRIC-treated areas were often located in the peripheral cornea. Corresponding regions were measured in each Sham eye. The 3 CCT and 3 PCT measurements in each frame were averaged together, before averaging data for each eye, time point, and treatment group. Two of the rabbits sacrificed 4 hours post-treatment were not imaged again before euthanasia, but were only measured pre- and immediately post-procedure. In the 1 month group, one rabbit's LIRIC-treated eye could not be measured post-operatively due to confounding swelling which arose from accidental damage caused by the patient interface during decoupling from the system after LIRIC. Because of this, her measurements were not included, dropping the number of LIRIC-treated eyes to 19 for the immediate post-treatment OCT measurements.

In-vivo confocal imaging—for the purpose of estimating central endothelial cell density was carried out as described previously (Huxlin *et al.*, 2013). Endothelial cell counts were performed over a 400×400 μm field of view (Cell Counter Plug-in, Image J, NIH, Bethesda, MD). Endothelial cells (red dots, Fig. 2B) were first tagged over a contiguous region in the field of view. The outline of this region was then traced (yellow line, Fig. 2B) to calculate its area and compute endothelial cell density (ECD). All 32 eyes were used to calculate the average, baseline ECD. For each cornea, at least five images per confocal scan (a total of 450 images) were measured to generate the average ECD. A total of 160 images were then analyzed pre-treatment; 290 images were analyzed post-treatment. As stated above, two rabbits from the 4 hour cohort were not imaged pre-euthanasia, and one rabbit's LIRIC-treated eye from the one month time period could not be measured immediately post-procedure due to confounding swelling (her data were thus removed from the immediate post-treatment average for ECD).

2.4 Tissue processing for histology

Histological assessments were designed to evaluate consequences of LIRIC and suction applanation on cell death, infiltration of inflammatory cells into the cornea, myofibroblast differentiation and corneal nerve distribution. Whether procedures induced cell death was assayed using terminal deoxynucleotidyl transferase-mediated dUTP-digoxigenin nick end labeling (TUNEL), which detects DNA fragmentation (Gao *et al.*, 1997; Helena *et al.*, 1998; Mohan *et al.*, 2003; Netto *et al.*, 2007; Wilson, 1997). Hematoxylin and eosin (H&E) staining was used to assess for the presence of inflammatory infiltrates (Lin *et al.*, 2015). To test for myofibroblast differentiation, which causes fibrosis and stromal haze (Jester *et al.*, 1999; Raviv *et al.*, 2000; Torricelli *et al.*, 2016), we used antibodies against alpha-smooth muscle actin (α-SMA). Finally, antibodies against neuron-specific class III beta-tubulin (TUJ-1) were used to stain corneal nerves (He *et al.*, 2010; Hindman *et al.*, 2019; Jeon *et al.*, 2018).

Rabbits were sacrificed at 4 hours, 2 weeks, 4 weeks, and 12 weeks after treatment. Four hours post-LIRIC provided valuable data concerning cells in the process of dying due to the procedure (Campos *et al.*, 1994; Gao *et al.*, 1997; Netto *et al.*, 2007; Watsky, 1995) but TUNEL was repeated at all timepoints to detect late-onset cell death. Myofibroblast differentiation was assayed at 2, 4 and 12 weeks post-procedure; if LIRIC was similar to

PRK, the density of α-SMA positive cells would be expected to peak somewhere from 2–4 weeks after LIRIC (Meltendorf *et al.*, 2007; Nien *et al.*, 2011; Torricelli *et al.*, 2016; Wilson *et al.*, 2001). By 12 weeks post-procedure, assuming that LIRIC was no worse than PRK in terms of inducing a fibrotic response, the cornea would be expected to return to a more quiescent state (Miyamoto *et al.*, 2003; Mohan *et al.*, 2003).

Rabbits were euthanized with an overdose of sodium pentobarbital (SomnaSol, Henry Schein Animal Health, Dublin, Ohio); the corneas were excised and immersion fixed in 1% paraformaldehyde/0.1M phosphate buffered saline (PBS), pH 7.4 for 10 minutes. They were then placed in a 30% sucrose/0.1 M PBS solution for 2 days at 4 °C. The corneas were embedded in Tissue Tek O.C.T. Compound (Sakura Finetek, Tokyo, Japan), frozen, and transversely sectioned into 20 μm-thick, serial sections using a cryostat (2800 Frigocut E, Reichert-Jung, Depew, NY). They were collected on gelatin-coated slides, then stored at −20 °C until staining. A total of 450 sections were collected for each eye to ensure that the 4.5 mm diameter pattern was completely sectioned. The LIRIC pattern was easily located in each corneal section because it auto-fluoresced green under 488 nm illumination, as previously described (Wozniak *et al.*, 2017; Yu *et al.*, 2019). Once located, 10 to 15 sequential slides (containing 3 corneal sections each) near the center of the pattern were chosen for TUNEL staining, H&E and immunohistochemistry.

TUNEL staining—The TUNEL assay was performed using the ApopTag® Red *In Situ* Apoptosis Detection Kit (S7165, Chemicon International, Millipore Inc., Temecula, CA) as described previously (Wozniak *et al.*, 2017). Once stained, slides were cover-slipped with mounting medium containing DAPI (VECTASHIELD®; Vector Laboratories, Burlingame, CA).

α-SMA staining: Corneal sections were first incubated with a mouse monoclonal anti-α-SMA antibody (Thermo Scientific #MS-113-P0; 1:400) overnight at 4 °C. The next day, slides were rinsed four times with 0.01 M PBS for 10 minutes at room temperature before secondary antibody was applied: AlexaFluor 555 conjugated to goat anti-mouse IgG (A21422, Invitrogen; 1:400). After incubation in the dark for 3 hours at room temperature, the slides were rinsed five times, away from the light, in 0.01 M PBS for 5 minutes at room temperature. Lastly, the slides were cover-slipped with mounting medium containing DAPI (VECTASHIELD®; Vector Laboratories, Burlingame, CA). The vascular walls in the limbal edge were used as positive controls as they naturally stain positively for α-SMA (Espana *et al.*, 2003).

H&E staining: was performed according to standard protocols on 3 corneal sections from each rabbit eye, all within the procedure area (i.e., inside the suction ring and/or LIRIC region).

TUJ-1 staining: Corneal sections were first incubated overnight at 4 °C with a mouse monoclonal TUJ-1 antibody (MMS-435P, Covance; 1:1000). After being rinsed four times with 0.01 M PBS for 10 minutes at room temperature, the secondary antibody, AlexaFluor 555 conjugated to goat anti-mouse IgG (A21422, Invitrogen; 1:400), was applied. The slides were dark-incubated for 3 hours at room temperature, rinsed five times with 0.01 M PBS for

5 minutes at room temperature, and cover-slipped with mounting medium containing DAPI (VECTASHIELD®; Vector Laboratories, Burlingame, CA).

Imaging and analysis of immuno-stained corneal sections: sections were selected for analysis if they had an intact epithelium and stroma, and if corneal integrity was preserved (*i.e.* no folds or large separations in the stromal layers). Slides from the same region of the cornea were chosen from the corresponding Sham eye, and the LIRIC region of interest (ROI) was superimposed. This ensured that the sections stained for the Sham eye had similar physical properties, and were located within the applanation zone.

All sections were imaged using an AX70 Olympus Microscope (Olympus Corporation, Tokyo, Japan) with a 10X microscope objective. We acquired photomicrographs of sequential, adjacent, non-overlapping, corneal sections with a high-resolution ORCA-Flash 4.0 LT Digital CMOS camera (Hamamatsu Photonics K.K., Shizuoka, Japan). The software used to capture images was either Q-Capture Pro 7 (QImaging, Surrey, BC, Canada) or HCImage (Hamamatsu Photonics K.K., Shizuoka, Japan) for TUNEL- and α-SMA-stained sections, or Neurolucida (MicroBrightField Biosciences, Williston, VT) for sections stained for TUJ-1. All sections were imaged with the appropriate combinations of fluorescent cubes (Semrock, Rochester, NY). LIRIC auto-fluoresced green under 488 nm excitation; TUNEL- and α-SMA-positive cells fluoresced red under rhodamine illumination as did TUJ-1-positive nerve fibers; DAPI-positive cells fluoresced blue under 350 nm illumination. Composite images were created using ImageJ or Neurolucida. A total of 39 α-SMA-stained and 65 TUNEL-stained sections were imaged for this study.

For TUJ-1-stained slides, we examined nerve distribution and quantified density separately for different corneal layers (epithelial, sub-basal, and stromal). Entire corneal sections were imaged and outlined using Neurolucida. The nerves in each complete corneal section were then manually traced in Neurolucida and color coded according to its layer location. If the eye had been treated with LIRIC, the GRIN pattern was also manually traced (Fig. 3). In these tracings, the area containing the LIRIC pattern was defined as the region of interest (ROI), and a box was drawn around it. The arc length of this segment was measured and normalized to the total corneal arc length. The beginning and ending locations of the LIRIC patterns were also normalized with respect to total arc length. Then, an identical ROI was created in the rabbit's corresponding Sham eye (Fig. 3B). This region was designed to have the same, normalized location and arc length as the ROI in the LIRIC-treated cornea. Within each ROI, the total nerve lengths for each layer of interest (epithelial, sub-basal, stromal) were measured, and the stromal and epithelial areas were calculated, allowing us to compute a nerve density index (NDI) for the epithelium and stroma as follows:

$$NDI_s = \frac{L_s}{A_s} \text{ and } NDI_e = \frac{L_e}{A_e} \quad (2)$$

where NDI_s is the stromal nerve density index, L_s is the total stromal nerve length, A_s is the stromal area, NDI_e is the epithelial nerve density index, L_e is the total epithelial nerve length, and A_e is the epithelial area (Jeon *et al.*, 2018).

The total sub-basal nerve length was normalized to the arc length of the relevant ROI. This was necessary because different corneal sections contained different lengths of LIRIC patterns; therefore, to accurately compare sub-basal nerve lengths, they had to be normalized to the measured ROI. The normalized sub-basal nerve length was computed as:

$$\hat{L}_{sb} = \frac{L_{sb}}{L_{BI}}, \tag{3}$$

where $\hat{L}_{sb}$ is the normalized sub-basal nerve length, L_{sb} is the total sub-basal nerve length, and L_{BI} is the arc length of the LIRIC pattern.

Finally, for the corneal nerve analysis, we also obtained four enucleated, Dutch Belted rabbit eyes from Covance Research Products to be used as unaltered controls (no LIRIC or suction-applanation was performed). These eyes were immersion fixed, sectioned, and stained for TUJ-1 in an identical fashion to the LIRIC-treated and Sham eyes. They were imaged and analyzed as described above. As with the Sham eyes, LIRIC ROIs were mapped onto unaltered corneal sections for a direct comparison (Fig. 3C). Since LIRIC patterns were located slightly temporally in the cornea, corneal sections from unaltered control eyes were analyzed across the entire cornea, not only the central region. From the *in vivo* rabbits, a total of 78 sections were stained for TUJ-1; 42 corneal sections were similarly stained and analyzed from unaltered control eyes.

Statistical analysis—When three or more intervention groups were compared, inter-group differences were assayed with one- or two-way ANOVAs. When only two groups were compared, two-tailed paired or unpaired Student's t-tests were performed. A probability of error of $p < 0.05$ was considered statistically significant.

3 Results

Immediately after writing, LIRIC patterns were visible due to a microbubble layer (Fig. 1D inset), which persisted for approximately 5 minutes. In the photograph shown in Fig. 1D, only the last three stitching zones are clearly visible, as the microbubble layer in the first two zones had already dissipated. Ten minutes after the procedure, the corneas were clear and transparent, and this persisted during the entire 12-week study. Sham eyes remained clear and transparent during the entire study.

3.1 Effect of LIRIC and Sham treatments on corneal thickness

Pre-operatively, OCT measurements of total corneal thickness showed no significant differences between rabbit eyes destined for LIRIC or Sham procedures, in either the central or peripheral cornea. A two-way ANOVA with repeated measures on corneal location (central/peripheral) showed no main effect of treatment group ($F_{(1,29)} = 0.23$, $p = 0.635$) or corneal location ($F_{(1,29)} = 1.29$, $p = 0.265$), and no interaction between the two ($F_{(1,29)} = 0.29$, $p = 0.594$). This confirmed relatively unbiased samples in the two treatment groups at baseline. Across all eyes examined (N = 32), central corneal thickness averaged (± SD) 366 ± 22 μm and peripheral thickness averaged 363 ± 25 μm.

However, corneal thicknesses decreased immediately after both LIRIC and Sham procedures (Fig. 4, Table 1). This was true for central cornea [Fig. 4G, Table 1, two-way repeated-measures ANOVAs: significant effect of time ($F_{(1,27)}$ = 46.97, p < 0.0001) but no effect of group (LIRIC/Sham, $F_{(1,27)}$ = 0.35, p = 0.559)], as well as for peripheral cornea (Fig. 4I, Table 1), where LIRIC patterns tended to be located [two-way repeated-measures ANOVAs: significant effect of time ($F_{(1,27)}$ = 77.32, p < 0.0001), but no main effect of group (LIRIC/Sham, $F_{(1,27)}$ = 0.03, p = 0.864)]. Because both LIRIC and Sham groups exhibited the same change post-procedure (a decrease in corneal thickness ~40 μm), we concluded that the corneal thinning observed was likely due to suction-applanation (which was performed identically in both groups) rather than the LIRIC writing. Moreover, while LIRIC patterns persisted in the cornea for all 12 weeks of follow-up, in the four eyes imaged 4 hours post-procedure (three LIRIC-treated and one Sham) both central and peripheral corneal thicknesses were no longer different from baseline [Fig. 4H, J; two-way repeated-measures ANOVA: no significant effect of time ($F_{(1,6)}$ = 0.86, p = 0.3895) or location (central/peripheral, $F_{(1,6)}$ = 0.04, p = 0.848)]. This remained true right up to 12 weeks post-LIRIC [Fig. 4H, J; two-way repeated-measures ANOVA: no main effect of time ($F_{(1,8)}$ = 1.26, p = 0.294) or corneal region (central/peripheral, $F_{(1,8)}$ = 0.35, p = 0.570)].

3.2 Effect of LIRIC on endothelial cell density

Pre-operative measurements of endothelial cell density were obtained for all 32 eyes used in the study through *in vivo* confocal imaging. Analysis of these measurements showed no statistical difference between eyes destined for the two treatment groups [unpaired, two-tailed Student's t-test: p = 0.866]. This confirmed the relatively unbiased nature of the rabbit cohort for ECD measurements at baseline. The average (± SD) ECD for all eyes was 2,874 ± 239 cells/mm^2.

No change in cell layer integrity was observed using *in vivo* confocal microscopy at any time point following LIRIC or Sham treatment. Representative photomicrographs from LIRIC-treated corneas are shown in Fig. 5A-F. Consistent with this qualitative observation, no change in ECD was measured immediately post-treatment for either LIRIC or Sham eyes [Table 2, Fig. 5G; two-way repeated measures ANOVA: no significant effect of time ($F_{(1,28)}$ = 2.64, p = 0.115), nor treatment (LIRIC/Sham: $F_{(1,28)}$ = 0.02, p = 0.889), nor an interaction between the two ($F_{(1,28)}$ = 0.01, p = 0.921)]. This lack of significant difference from baseline persisted at all subsequent time points (4 hours, 2 weeks, 4 weeks, and 12 weeks) post-treatment both in LIRIC-treated [Fig. 5H, one-way, independent ANOVA: $F_{(4,31)}$ = 0.78, p = 0.547] and Sham eyes [one-way, independent ANOVA: $F_{(4,15)}$ = 0.55, p = 0.702].

3.3 Biological effects of LIRIC

Cell death: In LIRIC-treated eyes, TUNEL-positive cells were only evident in the stroma 4 hours after the procedure (Fig. 6B). They were not seen in Sham eyes (Fig. 6A), nor in LIRIC-treated eyes at other time points examined (e.g. Fig. 6C). When present, TUNEL-positive cells were strictly co-located with zones of green autofluorescence indicative of the LIRIC pattern, extending no more than 5–10 μm from it in any direction. No positive cells were ever observed in the epithelium or endothelium, nor were they observed peripheral to

the LIRIC region, which is relevant because the applanation zone was larger than the laser-treated area.

Inflammatory response: Qualitative examination of all LIRIC and Sham eyes identified only a few, isolated cells in a few sections with the multi-lobal nuclear morphology of a neutrophil, the round, darkly-stained nuclei of lymphocytes. No cells with the orange-colored inclusions normally denoting macrophages were observed. We conclude that neither LIRIC nor suction-applanation induced a significant inflammatory response in rabbit corneas.

Myofibroblast differentiation: All Sham and LIRIC-treated eyes from the 2, 4, and 12-weeks timepoints were negative for α-SMA, a well-known marker of myofibroblast transformation and corneal fibrosis (Fig. 6D-F). As with TUNEL-staining, although the applanation zone was larger than the laser-affected, LIRIC zone, no regions of any of the corneas, Sham or LIRIC-treated, were α-SMA-positive.

Corneal nerve distribution: Both qualitative examination (Fig. 7A-C) and quantitative comparison (Table 3, Fig. 7D-F) between LIRIC, Sham, and unaltered [Control] corneal sections stained with TUJ-1 antibodies revealed that neither LIRIC nor Sham treatments altered corneal nerve distributions in the epithelial, sub-basal, or stromal layers at any time point following treatment.

One-way, independent ANOVAs comparing Control eyes with LIRIC- and Sham-treated eyes at four hours showed no significant effect of treatment group on NDIe ($F_{(2,8)} = 9.02$, $p = 0.345$), normalized sub-basal nerve length ($F_{(2,8)} = 2.18$, $p = 0.176$), or NDIs ($F_{(2,8)} = 1.52$, $p = 0.276$). Similarly, there was no significant effect on any nerve metric at 2 weeks (NDIe: $F_{(2,8)} = 1.05$, $p = 0.394$; normalized sub-basal nerve length: $F_{(2,8)} = 0.59$, $p = 0.577$; NDIs: $F_{(2,8)} = 0.22$, $p = 0.807$). At 12 weeks, one-way independent ANOVAs showed no significant effect of treatment on normalized sub-basal nerve length ($F_{(2,8)} = 3.62$, $p = 0.070$) or NDIs ($F_{(2,8)} = 0.19$, $p = 0.830$), but did show a significant effect on NDIe ($F_{(2,8)} = 5.99$, $p = 0.022$). However, paired, two-tailed Student's t-tests between treated and Control eyes at 12 weeks showed no significant effect on NDIe for both LIRIC-treated ($p = 0.899$) or Sham eyes ($p = 0.071$).

4 Discussion

The present study assessed - for the first time - the impact of a large-zone LIRIC, GRIN refractive corrector on corneal structure and biology *in vivo*. Unlike traditional laser refractive surgeries, LIRIC is non-incisional and non-ablative. Instead, it changes the stromal RI in a localized, customizable pattern to attain a desired refractive correction. The low-pulse-energy, high-repetition-rate laser process used for LIRIC works below the ablation threshold of the cornea, and the epithelium is left intact throughout the procedure. In *ex vivo* eyes, small LIRIC patterns induced minimal cell death, localized to the laser focal zone (Wozniak *et al.*, 2017). Here, we verified that larger patterns inscribed *in vivo*, also generated relatively few TUNEL-positive cells, also restricted to the laser focal zone. No subsequent TUNEL staining, nor myofibroblast differentiation were observed over ensuing

weeks. Finally, nerve distribution and densities, and endothelial cell densities remained unchanged, suggesting LIRIC to be the most biologically-neutral, laser-based, refractive correction technique to date.

4.1 Temporary decrease in corneal thickness is due to suction-applanation, not LIRIC

Prior work found no change in central corneal thickness 1 month after writing small (2.5 mm width), 3-layered, cylinder GRIN lenses into the corneas of live cats (Savage *et al.*, 2014). In the present study, we also observed no change in central or peripheral corneal thicknesses at 4 hours, 2, 4, or 12 weeks post-LIRIC. However, we did see a significant decrease in corneal thickness immediately after both LIRIC and Sham treatments. Because this outcome was observed in both laser-treated eyes and those undergoing suction applanation only, and because corneal thinning was measured outside as well as inside regions containing the LIRIC patterns, all within the applanation zone, we posit that suction applanation rather than LIRIC caused this temporary corneal thinning.

Equally notable was the lack of corneal swelling or cloudiness following our treatments, which is promising with regards to potential post-operative complications. Corneal edema can result from injury to the endothelium or epithelium (Baum *et al.*, 1984; Doughty and Cullen, 1990), but both were shown to be absent by our imaging and histological analyses.

4.2 LIRIC does not affect endothelial cell density

Endothelial cell health is a significant concern in laser exposures of the cornea. An important physiological function of this single cell layer is its ability to pump fluid and maintain proper corneal hydration (Baum *et al.*, 1984; Doughty and Cullen, 1990). If the endothelium is sufficiently compromised, its fluid permeability will increase, causing corneal edema (Lundberg *et al.*, 2005; Waring III *et al.*, 1982). Endothelial cells typically do not regenerate, and a sufficient loss of cells can cause endothelial cell density to drop below the threshold required to maintain proper fluid balance, compromising corneal transparency (Rao *et al.*, 1979). OCT findings showed no short- or long-term change in corneal thickness or bulk transparency following LIRIC or suction-applanation, suggesting that the endothelium remained healthy. This was confirmed by *in vivo* confocal imaging. Mean baseline ECD measured presently (~2,870 cells/mm^2) agreed well with published values for Dutch Belted rabbit corneas (Jones *et al.*, 2016), and neither LIRIC nor applanation caused significantly changes in these numbers at any of the time points examined.

Two main factors likely contributed to endothelial sparing following LIRIC: 1) the high NA in our focusing objective restricted the effective incident 405 nm laser light to a very thin layer of the mid-corneal stroma, and 2) pulse energies were in the nJ range, well below those used for ablation and flap creation (Aron-Rosa *et al.*, 1986; Netto *et al.*, 2007; Pettit *et al.*, 1995). The axial length of our focal volume was on the order of a few micrometers, with a Rayleigh range ~7 μm, and the endothelium was several hundred micrometers away from the focal plane. Therefore, light incident on the endothelium was highly diffuse compared to that in the focal volume due to the beam divergence resulting from the high NA. The resulting, dramatic reduction in energy density (at least 1000-fold), combined with the low pulse energy, resulted in no damage to endothelial cells.

4.3 LIRIC causes minimal, localized TUNEL staining

Consistent with prior findings *ex vivo* (Wozniak *et al.*, 2017), *in vivo* LIRIC caused minimal TUNEL staining, with positive cells restricted to the laser's focal region, where RI was changed. This is a reassuring outcome, as large amounts of cell death could cause an increased wound healing response and post-operative complications such as stromal haze and optical glare (Helena et al., 1998; Li et al., 2000; Mohan et al., 2003; Wilson, 2000, 2020a, b; Wilson and Kim, 1998).

Four hours after LIRIC, the TUNEL assay revealed only a single layer of positive cells, restricted to the LIRIC pattern. In comparison, femto-LASIK can ablate tens of micrometers of stromal material, and TUNEL-positive cells appear in the sub-ablation zone up to 150 μm below the flap (Campos *et al.*, 1994; Li *et al.*, 2000; Wozniak *et al.*, 2017). LASIK flaps also cause TUNEL-positive cells to appear in parts of the epithelium, and they damage the stromal-epithelial interface. Research has shown that an intact stromal-epithelial interface may be necessary to reduce the wound healing response associated with traditional laser refractive techniques (Nakamura *et al.*, 2001; Wilson, 2020a). Additionally, the magnitude of keratocyte apoptosis appears linked to a reduction in corneal transparency (Torricelli *et al.*, 2016). As such, LIRIC's minimal TUNEL positivity and lack of epithelial injury would be predicted to minimize myofibroblast differentiation and preserve corneal transparency.

4.4 LIRIC does not induce myofibroblast differentiation or inflammatory infiltration

The wound healing response that follows tissue removal with LASIK and PRK has been studied extensively and appears to underlie at least some of the post-operative complications observed following these procedures (Fan-Paul *et al.*, 2002; Mohan *et al.*, 2003; Netto *et al.*, 2005; Wilson, 1997, 2000, 2020b; Wilson and Kim, 1998). The number of myofibroblasts generated after PRK or LASIK in rabbit corneas is thought to be linked to the proximity of keratocytes to the treatment site and the severity of the damage to the epithelial basement membrane (Mohan *et al.*, 2003; Torricelli *et al.*, 2016). The limited cell death measured presently, coupled with the fact that LIRIC does not disrupt the epithelial-stromal interface suggests that a wound is not created in LIRIC. As such, one would not expect significant myofibroblast differentiation, and this was confirmed here, with a total lack of α-SMA staining. H&E staining also showed no infiltration of any part of the cornea by neutrophils, lymphocytes or macrophages, suggesting no significant inflammatory response. These results support our hypothesis that LIRIC should avoid many of the post-operative complications that can follow laser ablative techniques.

4.5 LIRIC does not affect corneal nerve distribution

The cornea is highly innervated, with corneal nerves responsible for registering discomfort, for controlling the blink reflex and tear production (Belmonte *et al.*, 2004; Marfurt *et al.*, 2010), all of which are necessary for corneal health and optical performance (Shaheen *et al.*, 2014). Current surgical vision correction techniques damage corneal nerves, which causes dry eye and patient discomfort, both of which are post-operative concerns (Ambrósio Jr *et al.*, 2008; Salomão *et al.*, 2009). In severe cases, corneal degeneration and blindness can result (Yamada *et al.*, 2008).

For the first time in the study of LIRIC, we have measured corneal nerve distribution over a period of three months in both LIRIC- and Sham-treated rabbit corneas. Unlike ablative laser refractive surgeries, LIRIC-treated eyes experienced no significant decrease in nerve density in any of the corneal layers they occupy (intra-epithelial, sub-basal or stromal) at any of the measured time points, when compared to unaltered/control eyes. Like the TUNEL response, this result is most likely attributable to the small laser interaction region used to create a localized RI change within the stroma. In addition, unlike keratocytes, on the rare occasions when the laser focal volume traversed stromal nerves, it appeared to leave them intact. In contrast, PRK destroys the epithelium and severs all the nerves it contains over a circular area ~8–9 mm in diameter. It also destroys sub-basal nerves, and because the laser ablation extends tens of micrometers into the anterior stroma, it ablates a good length of the stromal nerve trunks within the laser-treated area. PRK-treated eyes do not retain pre-operative corneal nerve densities, with only partial regeneration seen at 3 months (Hindman *et al.*, 2019; Jeon *et al.*, 2018; Medeiros *et al.*, 2018). LASIK flaps also damage epithelial, sub-basal nerves and stromal nerves, and this is before the additional damage sustained by stromal nerves from the laser ablation in the anterior stromal bed (Ma et al., 2014; Mohamed-Noriega et al., 2014). Studies have shown that the effects of denervation from LASIK are long-lasting, with decreased corneal nerve density persisting up to five years (Erie *et al.*, 2005; Liu *et al.*, 2020).

5 Conclusion

The present experiments represent the first study of the biological response to LIRIC *in vivo*, in a large, pre-clinical, animal model. LIRIC induced minimal cell death, evidenced by TUNEL staining, restricted to the thin region of RI change in the stroma. The epithelium and endothelium remained intact and TUNEL-negative. Corneal thickness and transparency were unchanged, and there was a complete lack of myofibroblast differentiation at all time points examined. Finally, normal corneal nerve distribution was also maintained in the epithelium, stroma, and sub-basal layer for up to three months post-treatment. Given these findings, LIRIC should improve upon the side-effect profile of current, photo-ablative techniques (Ambrósio Jr *et al.*, 2008; Erie *et al.*, 2005; Kato *et al.*, 1999; Mohan *et al.*, 2003). Overall, the present work suggests that LIRIC has significant potential as a safe, non-invasive procedure for human vision correction.

ACKNOWLEDGEMENTS AND FUNDING

The authors wish to thank Margaret DeMagistris and Christine Callan for animal anesthesia during LIRIC and Sham treatments, as well as for *in vivo* ocular imaging. We also thank Thurma McDaniel for tissue processing, histology, and expert immunohistochemistry.

Research reported in this publication was supported by NYSTAR through the University of Rochester's Center for Emerging and Innovative Sciences (CEIS), and a research grant from Clerio Vision, Inc. Funding was also provided by the National Eye Institute of the National Institutes of Health (R01 EY015836 and Core Grant P30 EY001319 to the Center for Visual Science) and an unrestricted grant to the University of Rochester's Department of Ophthalmology from the Research to Prevent Blindness Foundation (RPB). The content of this article is solely the responsibility of the authors and does not necessarily represent the official views of our granting agencies.

Abbreviations

α-SMA	alpha smooth muscle actin
AOM	acousto-optic modulator
CCT	central corneal thickness
DAPI	4’,6-diamidino-2-phenylindole fluorescent stain
ECD	endothelial cell density
FOV	field of view
GRIN	gradient index
GTI	Gires-Tournois interferometer
H&E	hematoxylin and eosin
IRIS	intra-tissue refractive index shaping
LASIK	laser in-situ keratomileusis
LIRIC	laser-induced refractive index change
NA	numerical aperture
OCT	optical coherence tomography
PBS	phosphate buffered saline
PCT	posterior corneal thickness
PRK	photorefractive keratectomy
RI	refractive index
ROI	region of interest
SHG	second harmonic generation
TUJ-1	neuron specific class III Beta-Tubulin
TUNEL	terminal deoxynucleotidyl transferase-mediated dUTP-digoxigenin nick end labeling

REFERENCES

Ambrósio R Jr, Tervo T, Wilson SE, 2008. LASIK-associated dry eye and neurotrophic epitheliopathy: pathophysiology and strategies for prevention and treatment. Journal of refractive surgery 24, 396–407. [PubMed: 18500091]

Aron-Rosa DS, Boulnoy JL, Carré F, Delacour J, Gross M, Lacour M, Olivo JC, Timsit JC, 1986. Excimer laser surgery of the cornea: qualitative and quantitative aspects of photoablation according to the energy density. Journal of Cataract & Refractive Surgery 12, 27–33. [PubMed: 3958947]

Baum J, Maurice D, McCarey B, 1984. The active and passive transport of water across the corneal endothelium. Experimental eye research 39, 335–342. [PubMed: 6499954]

Belmonte C, Acosta MC, Gallar J, 2004. Neural basis of sensation in intact and injured corneas. Experimental eye research 78, 513–525. [PubMed: 15106930]

Brooks DR, Brown NS, Savage DE, Wang C, Knox WH, Ellis JD, 2014. Precision large field scanning system for high numerical aperture lenses and application to femtosecond micromachining of ophthalmic materials. Review of Scientific Instruments 85, 065107.

Bühren J, Nagy L, Swanton JN, Kenner S, MacRae S, Phipps RP, Huxlin KR, 2009. Optical effects of anti-TGFβ treatment after photorefractive keratectomy in a cat model. Investigative ophthalmology & visual science 50, 634–643. [PubMed: 18952913]

Campos M, Szerenyi K, Lee M, McDonnell JM, Lopez PF, McDonnell PJ, 1994. Keratocyte loss after corneal deepithelialization in primates and rabbits. Archives of ophthalmology 112, 254–260. [PubMed: 8311779]

Chan A, Manche EE, 2011. Effect of preoperative pupil size on quality of vision after wavefront-guided LASIK. Ophthalmology 118, 736–741. [PubMed: 21093922]

Ding L, Blackwell R, Künzler JF, Knox WH, 2006. Large refractive index change in silicone-based and non-silicone-based hydrogel polymers induced by femtosecond laser micro-machining. Optics express 14, 11901–11909. [PubMed: 19529613]

Doughty MJ, Cullen AP, 1990. Long-term effects of a single dose of ultraviolet-B on albino rabbit cornea–II. Deturgescence and fluid pump assessed in vitro. Photochemistry and photobiology 51, 439–449. [PubMed: 2343062]

Erie JC, McLaren JW, Hodge DO, Bourne WM, 2005. Recovery of corneal subbasal nerve density after PRK and LASIK. American journal of ophthalmology 140, 1059–1064. e1051. [PubMed: 16376651]

Espana E, Ti S, Grueterich M, Touhami A, Tseng S, 2003. Corneal stromal changes following reconstruction by ex vivo expanded limbal epithelial cells in rabbits with total limbal stem cell deficiency. British journal of ophthalmology 87, 1509–1514.

Fan-Paul NI, Li J, Miller JS, Florakis GJ, 2002. Night vision disturbances after corneal refractive surgery. Survey of ophthalmology 47, 533–546. [PubMed: 12504738]

Gandara-Montano GA, Ivansky A, Savage DE, Ellis JD, Knox WH, 2015. Femtosecond laser writing of freeform gradient index microlenses in hydrogel-based contact lenses. Optical Materials Express 5, 2257–2271.

Gandara-Montano GA, Stoy V, Dudič M, Petrák V, Haškovcová K, Knox WH, 2017. Large optical phase shifts in hydrogels written with femtosecond laser pulses: elucidating the role of localized water concentration changes. Optical Materials Express 7, 3162–3180.

Gao J, Gelber-Schwalb TA, Addeo JV, Stern ME, 1997. Apoptosis in the rabbit cornea after photorefractive keratectomy. Cornea 16, 200–208. [PubMed: 9071534]

He J, Bazan NG, Bazan HE, 2010. Mapping the entire human corneal nerve architecture. Experimental eye research 91, 513–523. [PubMed: 20650270]

Helena MC, Baerveldt F, Kim W-J, Wilson SE, 1998. Keratocyte apoptosis after corneal surgery. Investigative Ophthalmology and Visual Science 39, 276–283. [PubMed: 9477983]

Hindman HB, DeMagistris M, Callan C, McDaniel T, Bubel T, Huxlin KR, 2019. Impact of topical anti-fibrotics on corneal nerve regeneration in vivo. Experimental eye research 181, 49–60. [PubMed: 30660507]

Huxlin KR, Hindman HB, Jeon K-I, Bühren J, MacRae S, DeMagistris M, Ciufo D, Sime PJ, Phipps RP, 2013. Topical rosiglitazone is an effective anti-scarring agent in the cornea. PloS one 8, e70785.

Jeon K-I, Hindman HB, Bubel T, McDaniel T, DeMagistris M, Callan C, Huxlin KR, 2018. Corneal myofibroblasts inhibit regenerating nerves during wound healing. Scientific reports 8, 12945. [PubMed: 30154512]

Jester JV, Petroll WM, Cavanagh HD, 1999. Corneal stromal wound healing in refractive surgery: the role of myofibroblasts. Progress in retinal and eye research 18, 311–356. [PubMed: 10192516]

Jones K, Choi J-H, Sponsel WE, Gray W, Groth SL, Glickman RD, Lund BJ, Reilly MA, 2016. Low-level primary blast causes acute ocular trauma in rabbits. Journal of neurotrauma 33, 1194–1201. [PubMed: 26393900]

Kato T, Nakayasu K, Hosoda Y, Watanabe Y, Kanai A, 1999. Corneal wound healing following laser in situ keratomileusis (LASIK): a histopathological study in rabbits. The British journal of ophthalmology 83, 1302. [PubMed: 10535863]

Kauffmann T, Bodanowitz S, Hesse L, Kroll P, 1996. Corneal reinnervation after photorefractive keratectomy and laser in situ keratomileusis: an in vivo study with a confocal videomicroscope. German journal of ophthalmology 5, 508–512. [PubMed: 9479547]

Li Q, Ashraf MF, Bekoe NA, Stark WJ, Chan C-C, O'Brien TPJGs.a.f.c., ophthalmology, e., 2000. The role of apoptosis in the early corneal wound healing after excimer laser keratectomy in the rat. 238, 853–860.

Lin A, Guo X, Inman RD, Sivak JM, 2015. Ocular inflammation in HLA-B27 transgenic mice reveals a potential role for MHC class I in corneal immune privilege. Molecular vision 21, 131. [PubMed: 25684978]

Liu YC, Jung ASJ, Chin JY, Yang LWY, Mehta JS, 2020. Cross-sectional Study on Corneal Denervation in Contralateral Eyes Following SMILE Versus LASIK. Journal of Refractive Surgery 36, 653–660. [PubMed: 33034357]

Lundberg B, Jonsson M, Behndig A, 2005. Postoperative corneal swelling correlates strongly to corneal endothelial cell loss after phacoemulsification cataract surgery. American journal of ophthalmology 139, 1035–1041. [PubMed: 15953433]

Ma K, Yan N, Huang Y, Cao G, Deng J, Deng Y, 2014. Effects of nerve growth factor on nerve regeneration after corneal nerve damage. International journal of clinical and experimental medicine 7, 4584. [PubMed: 25550989]

Marfurt CF, Cox J, Deek S, Dvorscak L, 2010. Anatomy of the human corneal innervation. Experimental eye research 90, 478–492. [PubMed: 20036654]

Medeiros CS, Marino GK, Lassance L, Thangavadivel S, Santhiago MR, Wilson SE, 2018. The impact of photorefractive keratectomy and mitomycin C on corneal nerves and their regeneration. Journal of Refractive Surgery 34, 790–798. [PubMed: 30540361]

Meltendorf C, Burbach GJ, Bühren J, Bug R, Ohrloff C, Deller T, 2007. Corneal femtosecond laser keratotomy results in isolated stromal injury and favorable wound-healing response. Investigative ophthalmology & visual science 48, 2068–2075. [PubMed: 17460262]

Miyamoto T, Saika S, Yamanaka A, Kawashima Y, Suzuki Y, Ohnishi Y, 2003. Wound healing in rabbit corneas after photorefractive keratectomy and laser in situ keratomileusis. Journal of Cataract & Refractive Surgery 29, 153–158. [PubMed: 12551683]

Mohamed-Noriega K, Riau AK, Lwin NC, Chaurasia SS, Tan DT, Mehta JS, 2014. Early corneal nerve damage and recovery following small incision lenticule extraction (SMILE) and laser in situ keratomileusis (LASIK). Investigative ophthalmology & visual science 55, 1823–1834. [PubMed: 24569584]

Mohan RR, Hutcheon AE, Choi R, Hong J, Lee J, Mohan RR, Ambrósio R, Zieske JD, Wilson SE, 2003. Apoptosis, necrosis, proliferation, and myofibroblast generation in the stroma following LASIK and PRK. Experimental eye research 76, 71–87. [PubMed: 12589777]

Nakamura K, Kurosaka D, Bissen-Miyajima H, Tsubota K, 2001. Intact corneal epithelium is essential for the prevention of stromal haze after laser assisted in situ keratomileusis. British journal of ophthalmology 85, 209–213.

Netto MV, Mohan RR, Ambrósio R Jr, Hutcheon AE, Zieske JD, Wilson SE, 2005. Wound healing in the cornea: a review of refractive surgery complications and new prospects for therapy. Cornea 24, 509–522. [PubMed: 15968154]

Netto MV, Mohan RR, Medeiros FW, Dupps WJ Jr, Sinha S, Krueger RR, Stapleton WM, Rayborn M, Suto C, Wilson SE, 2007. Femtosecond laser and microkeratome corneal flaps: comparison of stromal wound healing and inflammation. Journal of refractive surgery (Thorofare, NJ: 1995) 23, 667.

Nien CJ, Flynn KJ, Chang M, Brown D, Jester JV, 2011. Reducing peak corneal haze after photorefractive keratectomy in rabbits: prednisolone acetate 1.00% versus cyclosporine A 0.05%. Journal of Cataract & Refractive Surgery 37, 937–944. [PubMed: 21406325]

Patel SV, Erie JC, 2003. Aberrant regeneration of corneal nerves after laser in situ keratomileusis. Journal of Cataract & Refractive Surgery 29, 387–389. [PubMed: 12648654]

Peng MY, Hannan S, Teenan D, Schallhorn SJ, Schallhorn JM, 2018. Monovision LASIK in emmetropic presbyopic patients. Clinical Ophthalmology (Auckland, NZ) 12, 1665.

Pettit GH, Ediger MN, Weiblinger RP, 1995. Excimer laser ablation of the cornea. Optical Engineering 34, 661–667.

Rao G, Shaw E, Arthur E, Aquavella J, 1979. Endothelial cell morphology and corneal deturgescence. Annals of ophthalmology 11, 885–899. [PubMed: 496182]

Raviv T, Majmudar PA, Dennis RF, Epstein RJ, 2000. Mitomycin-C for post-PRK corneal haze. Journal of Cataract & Refractive Surgery 26, 1105–1106. [PubMed: 11041724]

Salomão MQ, Ambrósio R, Wilson SE, 2009. Dry eye associated with laser in situ keratomileusis: mechanical microkeratome versus femtosecond laser. Journal of Cataract & Refractive Surgery 35, 1756–1760. [PubMed: 19781472]

Savage DE, Brooks DR, DeMagistris M, Xu L, MacRae S, Ellis JD, Knox WH, Huxlin KR, 2014. First demonstration of ocular refractive change using blue-iris in live cats. Investigative ophthalmology & visual science 55, 4603. [PubMed: 24985471]

Shaheen BS, Bakir M, Jain S, 2014. Corneal nerves in health and disease. Survey of ophthalmology 59, 263–285. [PubMed: 24461367]

Shortt AJ, Allan BD, Evans JR, 2013. Laser-assisted in-situ keratomileusis (LASIK) versus photorefractive keratectomy (PRK) for myopia. Cochrane Database of systematic reviews.

Spadea L, Giammaria D, Trabucco P, 2016. Corneal wound healing after laser vision correction. British Journal of Ophthalmology 100, 28–33.

Torres LF, Sancho C, Tan B, Padilla K, Schanzlin DJ, Chayet AS, 2007. Early postoperative pain following Epi-LASIK and photorefractive keratectomy: a prospective, comparative, bilateral study. Journal of refractive surgery 23, 126–132. [PubMed: 17326351]

Torricelli AA, Santhanam A, Wu J, Singh V, Wilson SE, 2016. The corneal fibrosis response to epithelial–stromal injury. Experimental eye research 142, 110–118. [PubMed: 26675407]

Waring III GO, Bourne WM, Edelhauser HF, Kenyon KR, 1982. The corneal endothelium: normal and pathologic structure and function. Ophthalmology 89, 531–590. [PubMed: 7122038]

Watsky MA, 1995. Keratocyte gap junctional communication in normal and wounded rabbit corneas and human corneas. Investigative ophthalmology & visual science 36, 2568–2576. [PubMed: 7499079]

Wilson SE, 1997. Molecular cell biology for the refractive corneal surgeon: programmed cell death and wound healing. Journal of Refractive Surgery 13, 171. [PubMed: 9109075]

Wilson SE, 2000. Role of apoptosis in wound healing in the cornea. Cornea 19, S7–S12. [PubMed: 10832715]

Wilson SE, 2020a. Biology of keratorefractive surgery-PRK, PTK, LASIK, SMILE, inlays and other refractive procedures. Experimental Eye Research 198, 108136.

Wilson SE, 2020b. Corneal wound healing. Experimental eye research 197, 108089.

Wilson SE, Kim W-J, 1998. Keratocyte apoptosis: implications on corneal wound healing, tissue organization, and disease. Investigative Ophthalmology and Visual Science 39, 220–226. [PubMed: 9477978]

Wilson SE, Mohan RR, Mohan RR, Ambrósio R, Hong J, Lee J, 2001. The Corneal Wound Healing Response:: Cytokine-mediated Interaction of the Epithelium, Stroma, and Inflammatory Cells. Progress in retinal and eye research 20, 625–637. [PubMed: 11470453]

Wozniak KT, Elkins N, Brooks DR, Savage DE, MacRae S, Ellis JD, Knox WH, Huxlin KR, 2017. Contrasting cellular damage after Blue-IRIS and Femto-LASIK in cat cornea. Experimental eye research 165, 20–28. [PubMed: 28866013]

Wozniak KT, Germer TA, Butler SC, Brooks DR, Huxlin KR, Ellis JD, 2018. Scattering properties of ultrafast laser-induced refractive index shaping lenticular structures in hydrogels, Frontiers in

Ultrafast Optics: Biomedical, Scientific, and Industrial Applications XVIII. International Society for Optics and Photonics, p. 1052205.

Xu L, Knox WH, Huxlin KR, 2011. Exogenous and endogenous two-photon absorption for Intra-tissue Refractive Index Shaping (IRIS) in live corneal tissue [Invited]. Optical Materials Express 1, 1159–1164.

Yamada N, Matsuda R, Morishige N, Yanai R, Chikama T, Nishida T, Ishimitsu T, Kamiya A, 2008. Open clinical study of eye-drops containing tetrapeptides derived from substance P and insulin-like growth factor-1 for treatment of persistent corneal epithelial defects associated with neurotrophic keratopathy. British Journal of Ophthalmology 92, 896–900.

Yu D, Brown EB, Huxlin KR, Knox WH, 2019. Tissue effects of intra-tissue refractive index shaping (IRIS): insights from two-photon autofluorescence and second harmonic generation microscopy. Biomedical optics express 10, 855–867. [PubMed: 30800519]

Zheleznyak L, Butler SC, Cox IG, Huxlin KR, Ellis JD, Knox W, Waltz K, Vukich JA, Quesada G, Quesada R, 2019. First-in-human laser-induced refractive index change (LIRIC) treatment of the cornea. Investigative Ophthalmology & Visual Science 60, 5079–5079.

Highlights

- LIRIC is a multi-photon, non-ablative, fs-laser vision correction technique
- LIRIC works by changing the refractive index of the corneal stroma
- LIRIC does not disrupt the epithelium, endothelium or corneal nerve distribution
- Stromal keratocytes in the zone of refractive index change become TUNEL positive
- LIRIC does not induce fibrosis, inflammatory infiltration, nor changes in corneal structure
- The low biological impact of LIRIC suggests that it is a relatively safe method of vision correction

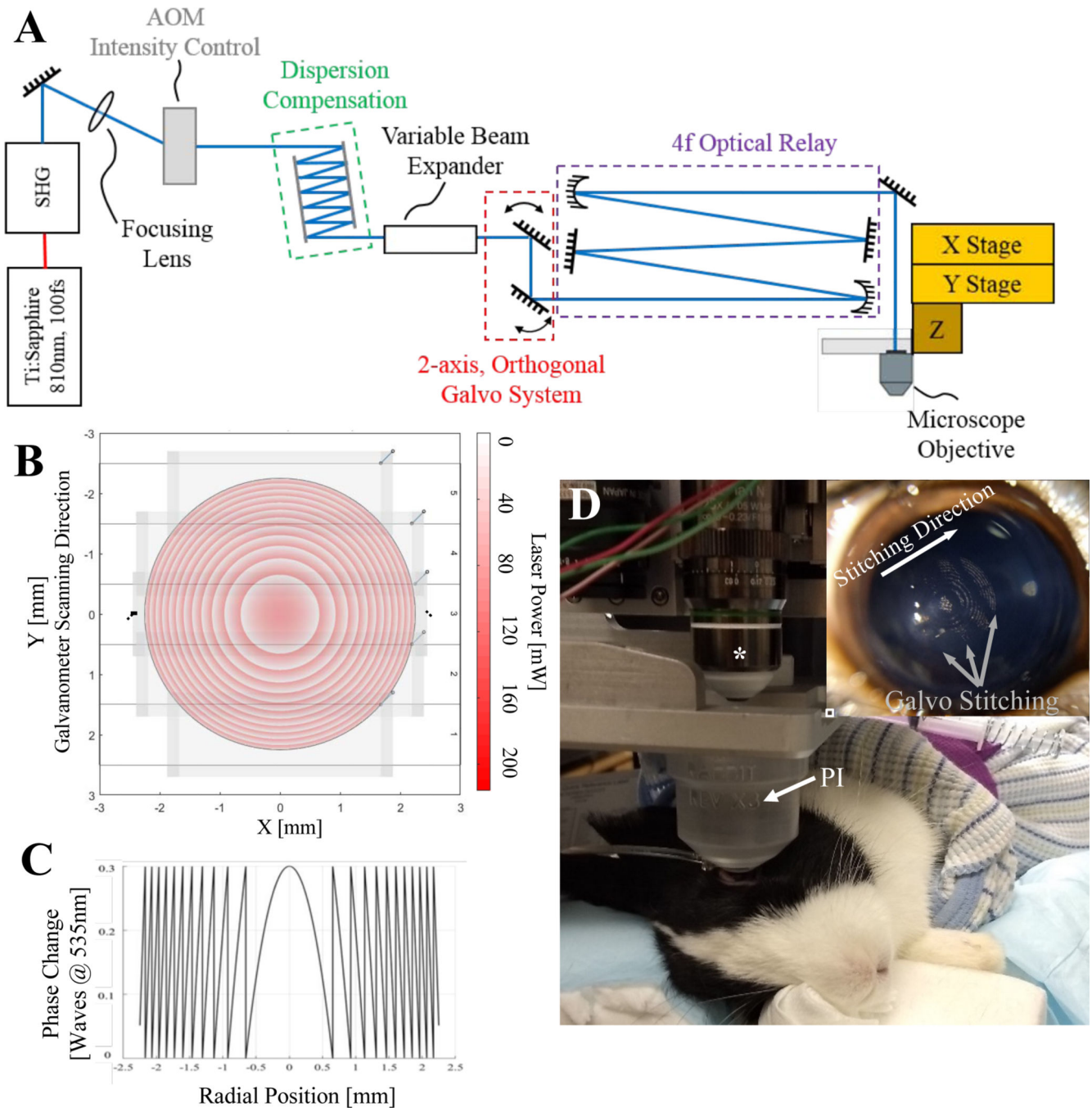

Figure 1. LIRIC instrumentation, patient positioning, and Fresnel lens pattern inscribed into the corneal stroma.

(A) A Ti:Sapphire oscillator produced 810 nm, 100 fs pulses which were frequency doubled to 405 nm. An acousto-optic modulator (AOM) was used to modulate the intensity of the laser in real-time. The beam bounced between two GTI mirrors for pulse compression. A variable beam expander controlled the NA, and a 4f relay was used to route the beam into the final scanning system. A two-axis, orthogonal galvanometer system, in conjunction with linear stages, was used to raster-scan the focal region within the cornea to create the LIRIC

structure. **(B)** Laser power profile of the phase map for the +2.5 D Fresnel lens structure written into rabbit eyes in the present study. The central region of the Fresnel lens had the highest laser dosage (darker red) and therefore, the largest induced phase change. Horizontal bands within the plot indicate stitching zones. **(C)** Plot showing induced phase change across a cross-section of the +2.5 D Fresnel lens shown in **B** at 0 mm on the Y-axis (black line in **B**). Maximum laser power was 200 mW, corresponding to a phase change measured in *ex vivo* corneas of ~0.3 waves at 535 nm. **(D)** Photograph of an anesthetized, Dutch-belted rabbit mounted into the laser system shown in **A** via the patient interface (PI) used to suction-applanate each cornea. The high-NA microscope objective (*) descended inside the PI to focus the laser beam into the mid-stromal region of the suction-applanated cornea. The inset shows a photograph of one rabbit eye immediately after LIRIC. The stitching direction is indicated, with the laser scanning direction being parallel. Note the Fresnel zones and the stitching bands, which are clearly visible while microbubbles are still present for a few minutes after the procedure.

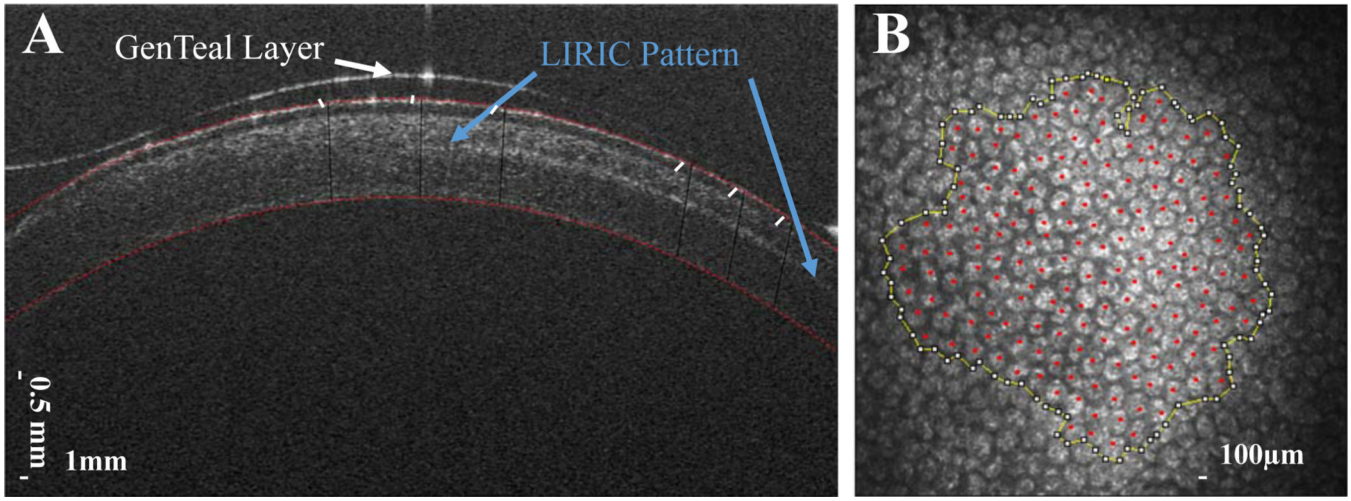

Figure 2. ***In vivo*** **imaging and analysis protocols.**

(A) OCT image of a rabbit eye treated with LIRIC. The LIRIC pattern was visible as a thin region of increased reflectivity – in this case, in the peripheral mid-stroma. Using a custom MATLAB program, corneal thickness was measured between two best fit circles (red dashed lines) denoting the anterior and posterior surfaces of the cornea. At each of three locations in the central and three locations in peripheral cornea (while lines), the program found a vector normal to the anterior surface, then analytically solved for the distance to the intersecting point with the posterior surface. **(B)** Confocal micrograph of the endothelium in a LIRIC-treated cornea. Cell counting analysis was performed in ImageJ. Cell density was estimated by measuring the area (encircled by yellow line) over which the cells (marked with red dots) were counted.

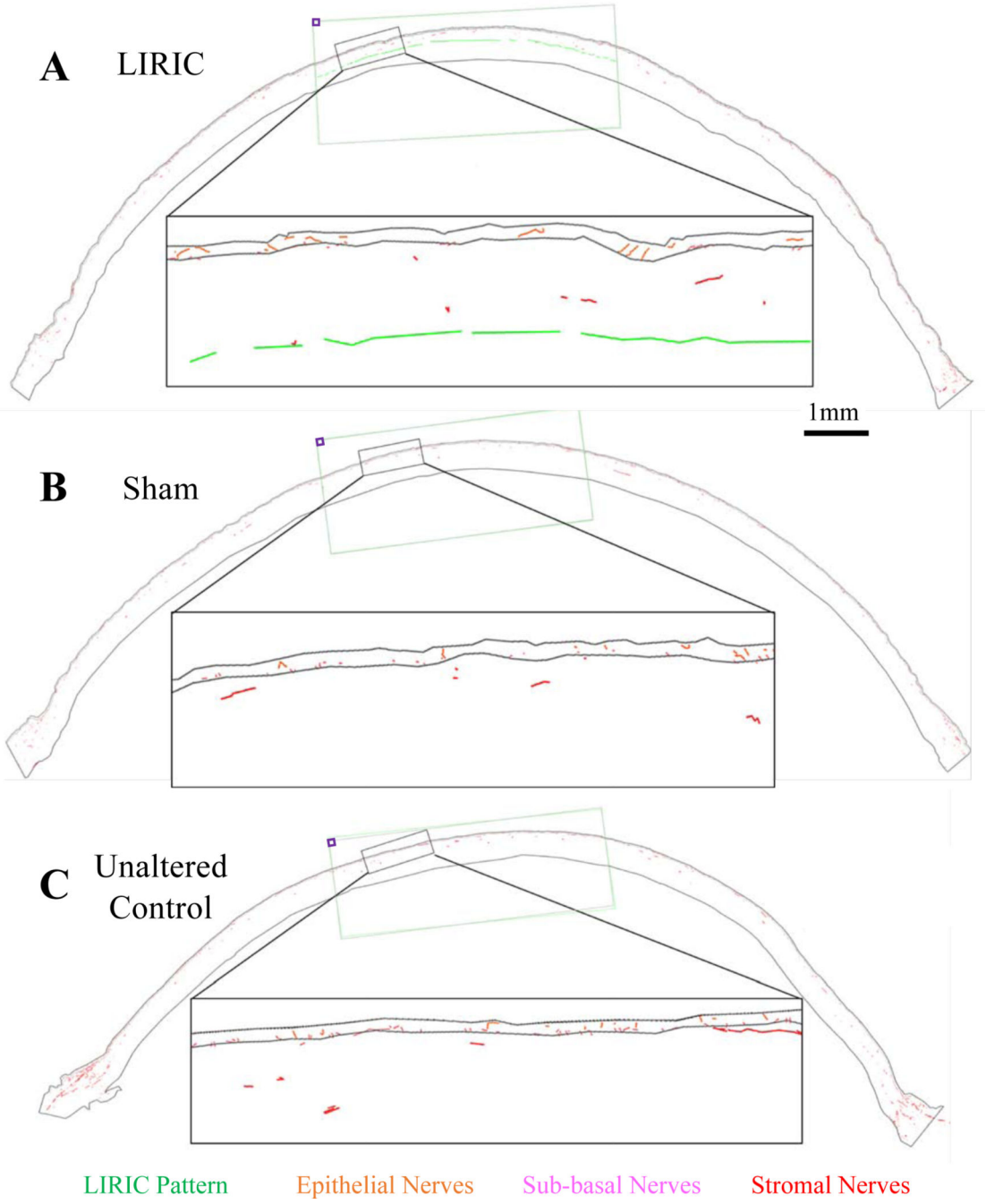

Figure 3. Corneal nerve reconstruction and analysis protocol.

Sample reconstructions of a LIRIC-treated cornea **(A)**, a Sham-treated cornea **(B)** and an unaltered, control rabbit cornea **(C).** Insets show traced nerves, which are color-coded in a region-specific manner. The LIRIC region was first defined on LIRIC-treated corneas (purple box in **A**), and it was then superimposed onto corresponding regions of Sham-treated and unaltered Control corneas for quantitative analysis. Nerve traces, as well as the stromal and epithelial area contained within the regions of interest were quantified in Neurolucida.

From these measurements, stromal and epithelial nerve densities were calculated, along with the sub-basal nerve length, normalized to the length of each LIRIC pattern.

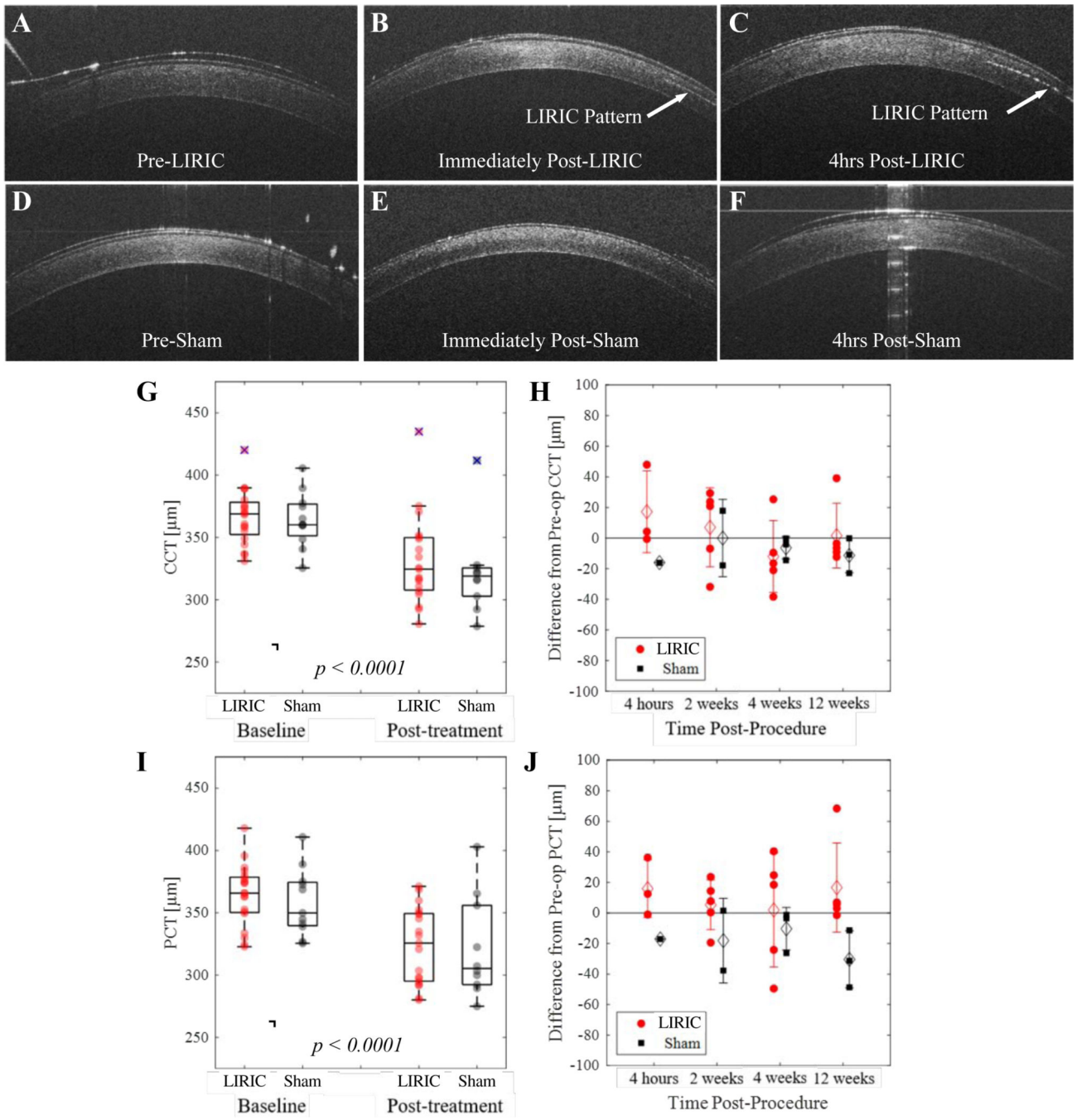

Figure 4. Impact of LIRIC and Sham treatments on corneal thickness.

OCT images of LIRIC-treated **(A-C)** and Sham eyes **(D-F)**. **(G)** Boxplots of central corneal thickness (CCT) prior to and immediately after LIRIC (red) or Sham (black) treatment. Each box represents the interquartile range, with the line denoting the median. The whiskers extend to the maximum and minimum values which are not outliers. Blue X denotes outliers (>1.5 times the interquartile range away from the edges of the box) in each group. P-values from two-way repeated measures ANOVA. **(H)** Plot of change in CCT from baseline LIRIC (red) or Sham (black)-treated eyes. Individual data (circles, squares) and means (diamond) ±

SD are provided at each time point. **(I)** Boxplots of peripheral corneal thickness (PCT) before and immediately after LIRIC or Sham treatment. Labeling conventions as in **G**. **(J)** Plot of change in PCT from baseline in LIRIC (red) or Sham (black)-treated eyes. Labeling conventions as in **H**. See main text for descriptive statistics.

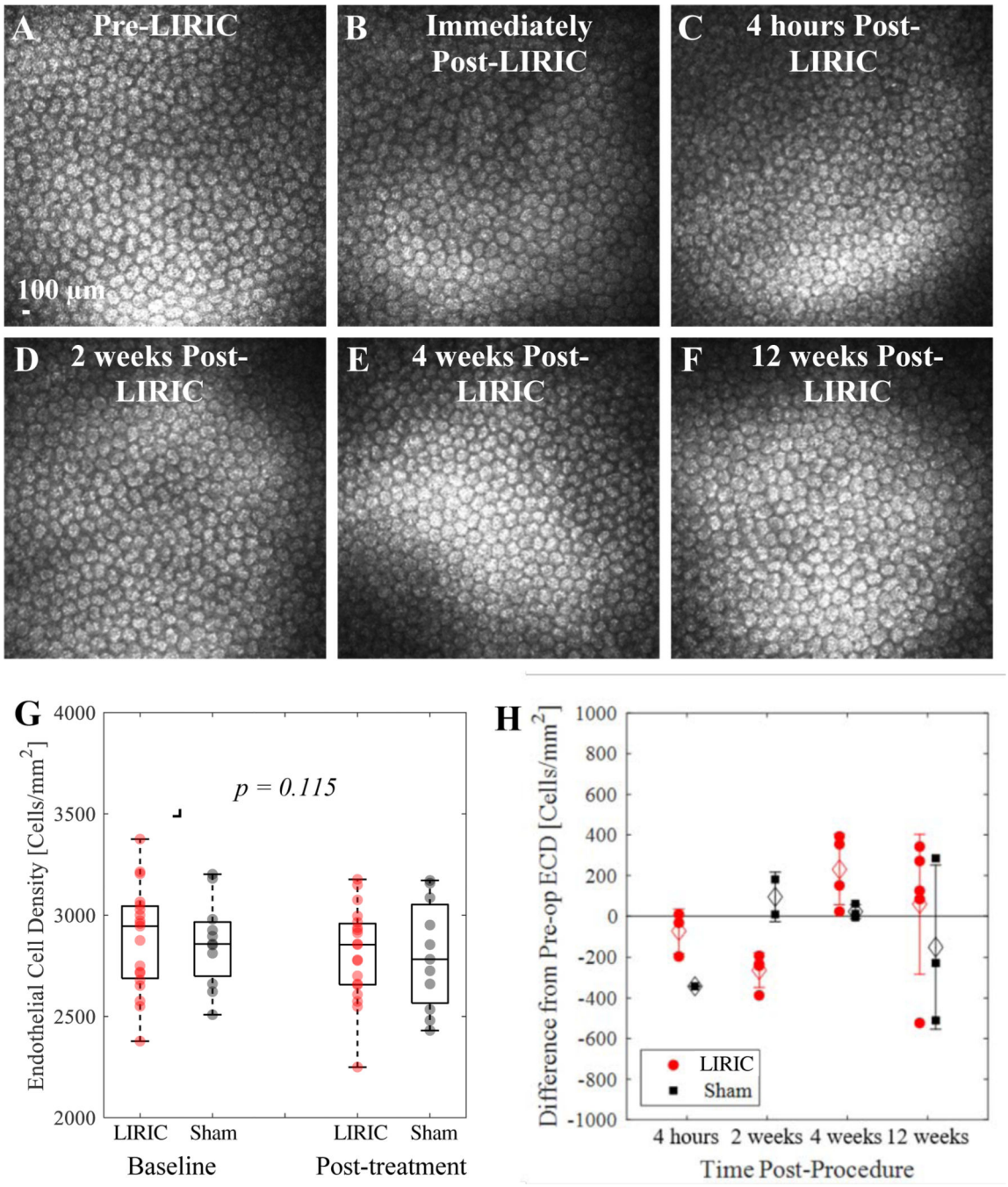

Figure 5. Impact of LIRIC and Sham treatments on endothelial cell density.

(A-F) Confocal images of LIRIC-treated rabbit corneas at various time points pre- and post-treatment. In all images, the endothelial cell layer appeared intact. Scale is the same for all micrographs. **(G)** Boxplots of endothelial cell densities before and immediately after treatment for LIRIC (red) or Sham eyes (black). The box represents the interquartile range with the line denoting the median value. P-values were computed from a two-way repeated measures ANOVA **(H)** Plot of change in endothelial cell density (ECD) relative to baseline

at various time points following treatments. Individual data (circles, squares) and means (diamond) ± SD are provided at each time point. See main text for full descriptive statistics.

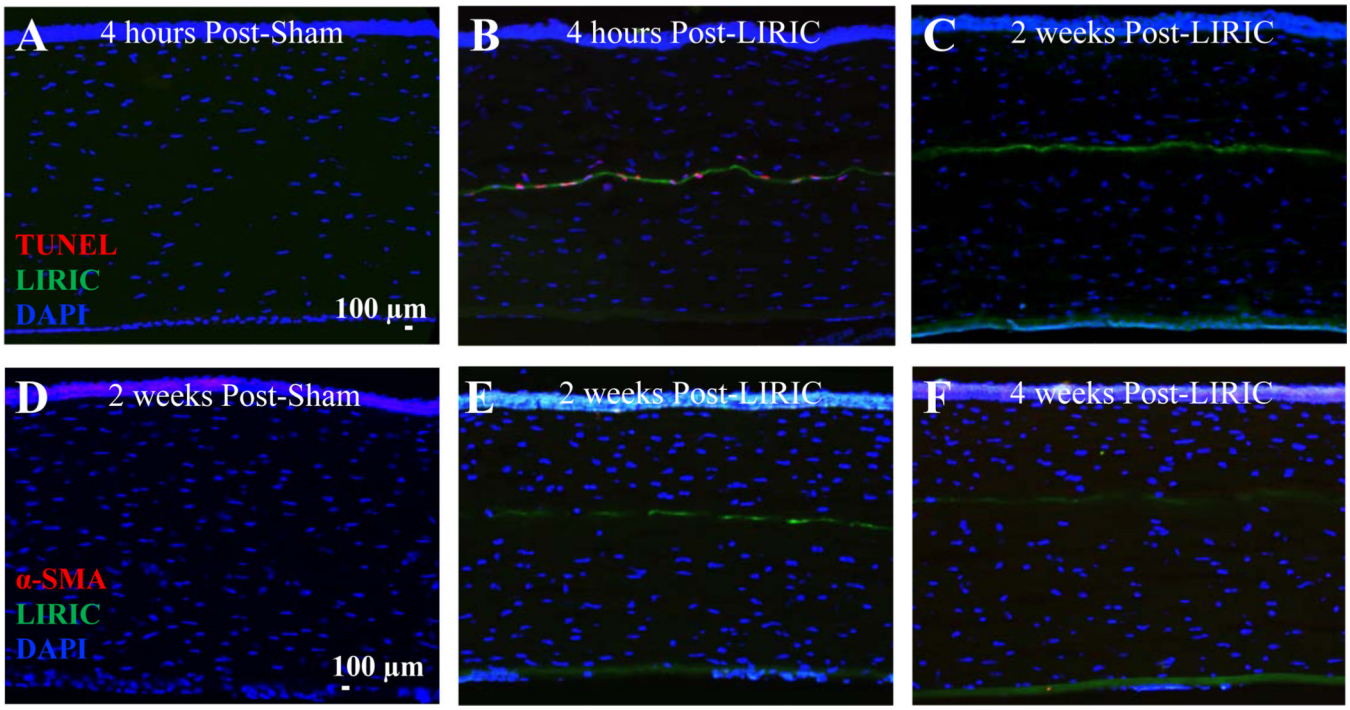

Figure 6. Impact of LIRIC and Sham treatments on cell death and myofibroblast differentiation.

(A) Corneal section from a Sham-treated rabbit eye 4 hours after suction-applanation, reacted for TUNEL (red fluorescence) and counterstained with DAPI (blue fluorescence). The epithelium is uppermost, and single-layer endothelium is located at the bottom of the photomicrograph. Note the lack of TUNEL-positive cells across this cornea. **(B)** Corneal section from a rabbit eye 4 hours after LIRIC. Staining and orientation are as in **A** except that green autofluorescence localizes the LIRIC pattern, a +2.5 D Fresnel lens. Photomicrographs are taken in the center of the pattern, in the largest Fresnel zone. Note the presence of TUNEL-positive cells across the entire pattern, but absent elsewhere. **(C)** Corneal section from a rabbit eye 2 weeks after LIRIC. Staining and orientation as in **B**. Note the lack of TUNEL-positive cells across the LIRIC pattern. In fact, no TUNEL-positive cells were seen in LIRIC-treated corneas after the 4-hour time point. **(D)** Corneal section from a Sham-treated rabbit eye 2 weeks after suction-applanation. The section was immuno-reacted with antibodies against α-SMA (red fluorescence) and counterstained with DAPI (blue fluorescence). There was complete absence of α-SMA staining in all Sham-treated corneas at all time points. **(E)** Corneal section from a rabbit eye 2 weeks after LIRIC. Staining and orientation as in **D** except that green autofluorescence denotes the LIRIC pattern. **(F)** Corneal section from a rabbit eye 4 weeks after LIRIC. Staining and orientation as in **E**. No α-SMA-positive regions were ever seen in at any time point, in either Sham- or LIRIC-treated corneas.

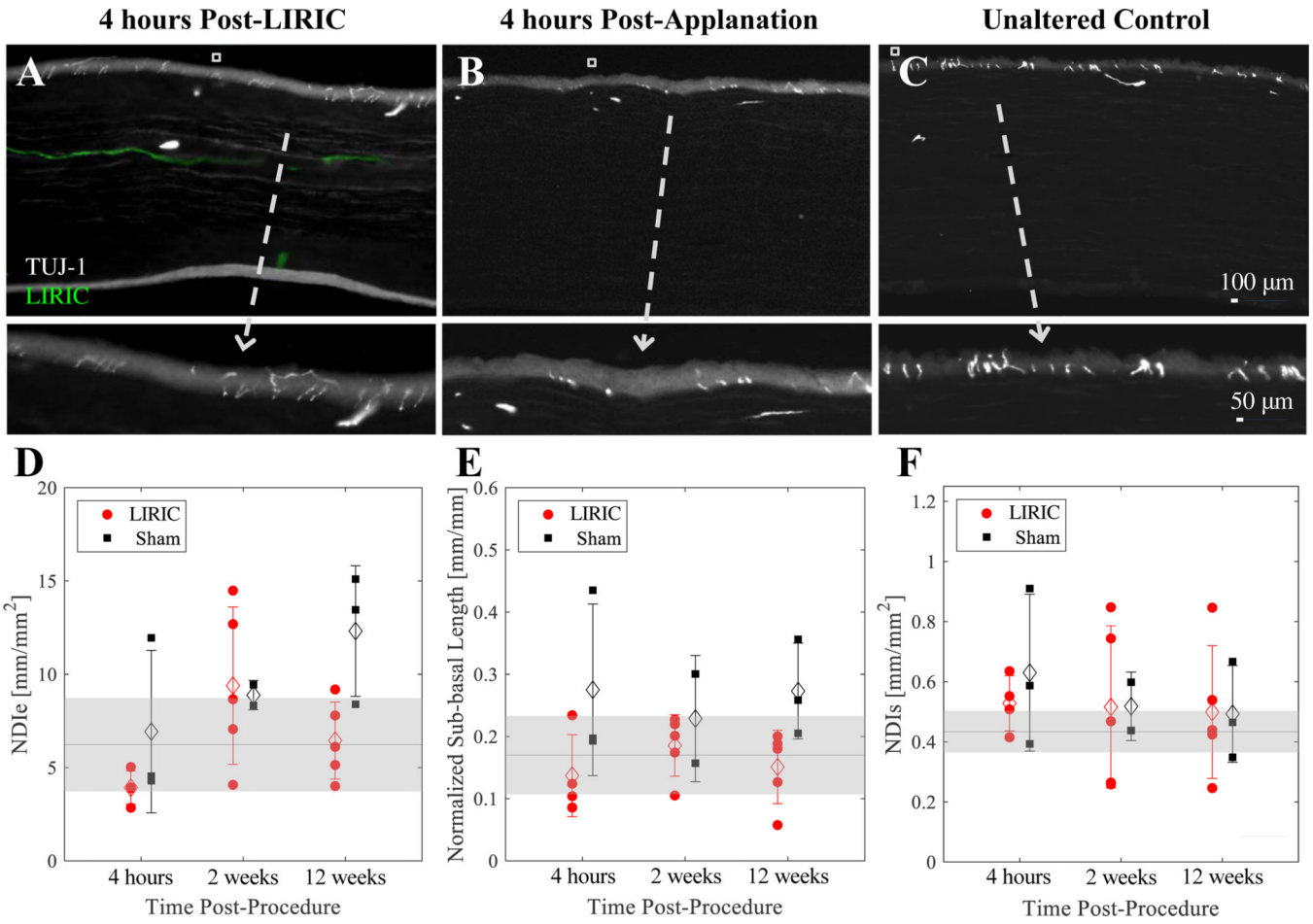

Figure 7. Effect of LIRIC and Sham treatments on corneal nerve distribution.

(A) Photomicrograph of a corneal section from an animal sacrificed 4 hours after LIRIC and immuno-stained with TUJ-1 antibodies (LIRIC pattern is false-colored green). The inset highlights a region of the epithelium (uppermost, grey layer in both photographs) containing a relatively high density of corneal nerve endings. **(B)** Photomicrograph of a corneal section 4 hours after Sham treatment, stained identically to **A**. **(C)** Corneal section from an unaltered, Control eye, stained identically to **A** and **B**. Note the similar distribution and density of corneal nerves in all 3 groups. **(D)** Plot of epithelial nerve density index (NDIe) at different time points after LIRIC or Sham treatment. Individual measurements (circles/squares) and mean ± SD (diamonds) are shown. Black line and grey zone denote the mean ± SD obtained from unaltered, Control eyes. **(E)** Plot of normalized sub-basal nerve length at different time points after LIRIC or Sham treatment. Labeling conventions as in **D**. **(F)** Plot of stromal nerve density index (NDIs) at different time points after LIRIC or Sham treatment. Labeling conventions as in **D** and **E**. There was a lack of significant change in corneal nerve lengths and densities following both LIRIC and Sham treatment relative to unaltered, Control rabbit corneas. Descriptive statistics are provided in the main text.

Table 1.

Central and peripheral corneal thicknesses of rabbit corneas before and immediately after treatment.

Both central and peripheral corneal thicknesses decreased immediately after LIRIC and suction applanation (Sham). Descriptive statistics are provided in the text. The number of eyes analyzed (n) is indicated for each cohort. SD = standard deviation of the mean.

Central Corneal Thickness [μm] *Mean ± SD*			**Peripheral Corneal Thickness [μm]** *Mean ± SD*		
Pre- Treatment (*n* = *32*)	**Post- LIRIC (*n* = *19*)**	**Post- Sham (*n* = *11*)**	**Pre- Treatment (*n* = *32*)**	**Post- LIRIC (*n* = *19*)**	**Post- Sham (*n* = *11*)**
367 ± 22	*331 ± 36*	*321 ± 35*	*364 ± 25*	*323 ± 31*	*321 ± 41*

Table 2.

Endothelial cell densities before and immediately after treatment.

There was no statistically significant change in endothelial cell density immediately after treatment for LIRIC and Sham eyes. Descriptive statistics are provided in the text. The number of eyes analyzed (n) is indicated for each cohort. SD = standard deviation of the mean.

Endothelial Cell Density [cells/mm^2]		
Mean* ± *SD		
Pre-Treatment *(n = 32)*	**Post-LIRIC *(n = 19)***	**Post-Sham *(n = 11)***
2,871 ± 243	2,810 ± 231	2,803 ± 266

Table 3.

Impact of LIRIC and Sham treatments on corneal nerve lengths and densities.

The number of eyes analyzed (n) is indicated for each cohort. All values are means ± standard deviation.

Epithelial Nerve Density Index [mm/mm^2]			
	4 hours	**2 weeks**	**12 weeks**
Control (*n = 4*)	6.22 ± 2.50	--	--
LIRIC (*n = 15*)	3.93 ± 0.89	9.39 ± 4.22	6.45 ± 2.06
Sham (*n = 8*)	6.93 ± 4.35	8.88 ± 0.79	12.32 ± 3.50

Normalized Sub-basal Nerve Length [mm/mm]			
	4 hours	**2 weeks**	**12 weeks**
Control (*n = 4*)	0.17 ± 0.06	--	--
LIRIC (*n = 15*)	0.14 ± 0.07	0.19 ± 0.04	0.15 ± 0.06
Sham (*n =8*)	0.27 ± 0.14	0.23 ± 0.10	0.27 ± 0.08

Stromal Nerve Density Index [mm/mm^2]			
	4 hours	**2 weeks**	**12 weeks**
Control (*n = 4*)	0.43 ± 0.07	--	--
LIRIC (*n = 15*)	0.53 ± 0.09	0.52 ± 0.27	0.50 ± 0.22
Sham (*n = 8*)	0.63 ± 0.26	0.52 ± 0.11	0.49 ± 0.16